# Sequential generation method for hexagonal lattice shells with edge offset mesh

Ryo WATADA[*], Makoto OHSAKI[a]

[*]Department of Architectural and Environmental Design, Osaka Sangyo University, Japan
3-1-1 Nakagaito, Daito, Osaka, 574-8530, Japan
watada@edd.osaka-sandai.ac.jp

[a] Department of Architecture and Architectural Engineering, Kyoto University, Japan

## Abstract

In this study, we propose a procedure using sequential optimization to find a hexagonal edge offset (EO) mesh that consists only of straight beams with the same height, approximates a specified surface shape, avoids twisting and misalignment at the joints, and maintains planarity in its hexagonal faces. The optimization problem determines the EO mesh by minimizing the angle between the node axis and the normal vector at the nearest point on the specified surface, while maintaining parallelity to the Koebe mesh, which is obtained from the Möbius transformation of packed circles on the unit sphere, a necessary and sufficient condition for EO mesh. Here, the design variables of the optimization problem are the lengths of each edge of the EO mesh, and the optimization is repeated for addition of one or several faces. The maximum distance between each node of the resulting mesh and the specified surface is considered as a constraint. The obtained mesh is an EO mesh where all edge offset values are strictly constant and the planarity of each face and beam is maintained. The effectiveness of the proposed method is demonstrated through the first numerical example applied to various surfaces with positive Gaussian curvature, and the second numerical example applied to rotational surfaces with fixed edge normal vectors. The second example shows that, by combining this method with structural analysis, it is possible to generate lattice shells that excel in both constructability and mechanical properties.

*Keywords*: edge offset mesh, mesh offset, hexagonal lattice shell, Möbius transformation, torsion-free node, optimization

## 1. Introduction

Lattice shells, used extensively in architectural roof design, are structures made from straight lattice beams. They can be viewed as a combination of a polygonal mesh M and its corresponding offset mesh M′, as depicted in Fig. 1, to represent beam heights. Mesh M is formed from nodes $x_i \in \mathbb{R}^3$ and edges $e_{ij}$, while the offset mesh M′ comprises an equivalent set of offset nodes $x_i'$ and offset edges $e_{ij}'$. A *node axis* $A_i$ is defined as the line connecting $x_i$ and $x_i'$. A *central plane*, described in [1], is formed by two edges $e_{ij}$ and $e_{ij}'$, and two node axes $A_i$ and $A_j$, representing the symmetry plane of a lattice beam.

Lattice shell structures often has several geometric construction challenges, as illustrated in Fig. 2. Geometric torsion, depicted in Fig. 2(a), arises when all central planes of the connecting beams do not join in a single node axis. Fig. 2(b) demonstrates the kinks caused by differences in the vertical angles between the node axis and the central axes of the beams. The creation of a mesh with planar faces that are free from torsion and kinks is crucial for reducing construction costs and time.

An *edge offset mesh (EO mesh)* is a offset mesh in which the distance of corresponding parallel edges $e_{ij}$ and $e_{ij}'$ equals $d$ for every edge [1]. It is known that a latticed shell composed of EO mesh has planar faces with no geometric torsion and kink. It is known that a mesh M is EO mesh if and only if M is

parallel with a *Koebe mesh* K, which are generated from circles packed on a sphere. Additionally, it is also known that Möbius transformations preserve the tangency between adjacent circles [2].
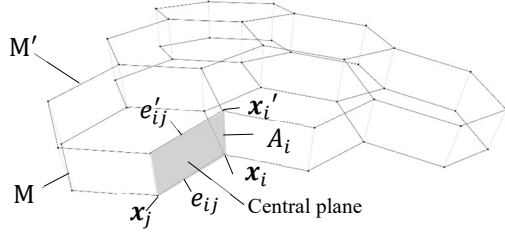


Figure 1. Mesh M and its offset mesh M′ determining quadrilateral central planes describing the symmetry planes of the beams
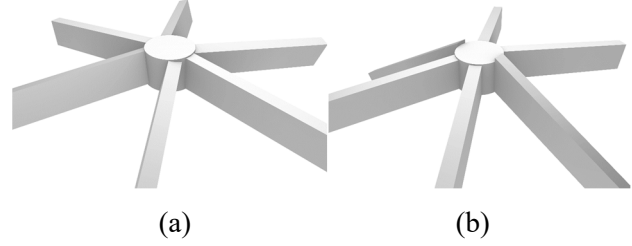


Figure 2. (a) A node with geometric torsion, (b) Kinks due to variation of vertical angles

Pottmann et al. [1] introduced an optimization method to generate EO meshes from Koebe meshes. This approach involves using the EO mesh nodal coordinates and those of the corresponding Koebe mesh as optimization variables, focusing on minimizing the distance to a reference surface and optimizing a fairness function of the mesh. The requirements for the meshes to have planar faces and to be parallel to the Koebe mesh are enforced through penalty functions included in the objective functions, ensuring the meshes achieve an approximately constant edge distance (approximate edge offset). They also demonstrated that the proposed method is effective in generating EO meshes along surfaces with negative Gaussian curvature by using concave polygons on each face.

In this study, we propose a procedure using sequential optimization to find a hexagonal EO mesh that consists only of straight beams with the same height, approximates a specified surface shape, avoids twisting and misalignment at the joints, and maintains planarity in its hexagonal faces. The optimization problem determines the EO mesh by minimizing the angle between the node axis of the EO mesh and the normal at the nearest point on the specified surface, while maintaining parallelism with the Koebe mesh, which is obtained from the Mobius transformation of packed circles on the unit sphere, a necessary and sufficient condition for EO mesh. Here, the design variables of the optimization problem are the lengths (or the coefficients that determine these lengths) of each edge in several faces of the EO mesh, and the optimization is repeated for addition of one or several faces. The maximum distance between each node of the resulting mesh and the specified surface is considered as a constraint. The obtained mesh is an EO mesh where all edge offsets are strictly constant and the planarity of each face and beam is maintained. The effectiveness of this method on various surfaces with positive Gaussian curvature is demonstrated through numerical examples.

Additionally, this method is applied to parametric rotational surfaces with fixed normal directions at the outer edges, proposing a shape design method for EO lattice shells that are dome-shaped and have excellent constructability. By using a Koebe mesh that conforms to the normal direction of the surface at the outer edge, it is demonstrated that lattice shells satisfying the properties of EO meshes and fitting the shape of the specified surface can be parametrically generated. Furthermore, by combining this method with structural analysis, it is shown through numerical examples that it is possible to generate lattice shells that has high constructability and mechanical properties.

## 2. Methodology

### 2.1. Generating Koebe mesh by Möbius transformation

Consider $z \in \mathbb{C}$ as a complex variable. A Möbius transformation on the complex plane is expressed as

$$f(z) = \frac{az+b}{cz+d} \quad (a,b,c,d \in \mathbb{C}, ad - bc \neq 0) \tag{1}$$

$$= \rho e^{i\theta} \left( \frac{1}{z+\alpha} + \beta \right) \tag{2}$$

where $\alpha$ and $\beta$ are complex numbers, $\rho$ is a positive real number, $\theta$ is a real number satisfying $-\pi \leq \theta < \pi$ and $i$ is the imaginary unit. Here we ignore the parameter $\theta$, which only concerns rotation around the origin ($Z$-axis). Then, assuming $\alpha = \alpha_R + i\alpha_I$ and $\beta = \beta_R + i\beta_I$, the Möbius transformation can be determined by five real parameters $\alpha_R, \alpha_I, \beta_R, \beta_I$ and $\rho$ which we called *Möbius transformation parameters*. By defining the base circle pattern $P_0$ on the *XY* plane and the Möbius transformation parameters, the corresponding Koebe mesh K on the unit sphere can be determined. For more details, see Watada and Ohsaki [3].

## 2.2. Sequential face generation of EO mesh

When a Koebe mesh K on the unit sphere is given, an EO mesh M can be defined as a parallel mesh to K, as shown in Fig. 3. In this study, we propose a sequential face generation method of EO mesh keeping the parallelity to the Koebe mesh as shown in Fig. 4. Here, each face of the EO mesh M, except for the first one, is sequentially generated in such a way that it is adjacent to the already existing faces. The number of parameters for the face generation method depends on the number of neighboring faces:

1. If the number of neighboring faces is one, the new face $f$ can be defined by two edge length parameters $\xi_{f1}$ and $\xi_{f2}$, and one edge length ratio parameter $\eta_f$ as shown in Fig. 4(a).

2. If the number of neighboring faces is three, the new face $f$ can be defined by one parameter $\eta_f$ as shown in Fig. 4(b).

3. If the number of neighboring faces is two, the new face $f$ can be defined by two parameters $\xi_{1f}$ and $\eta_f$ as shown in Fig. 4(c).
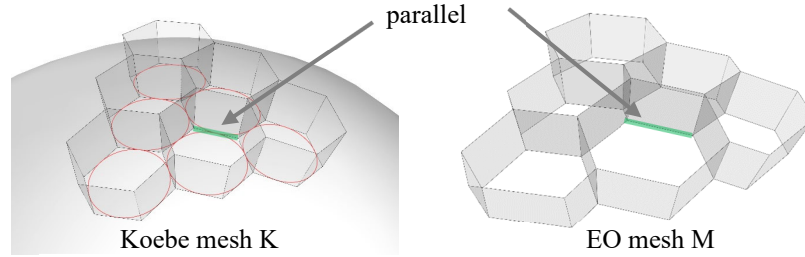


Figure 3. EO mesh as a parallel mesh of a Koebe mesh
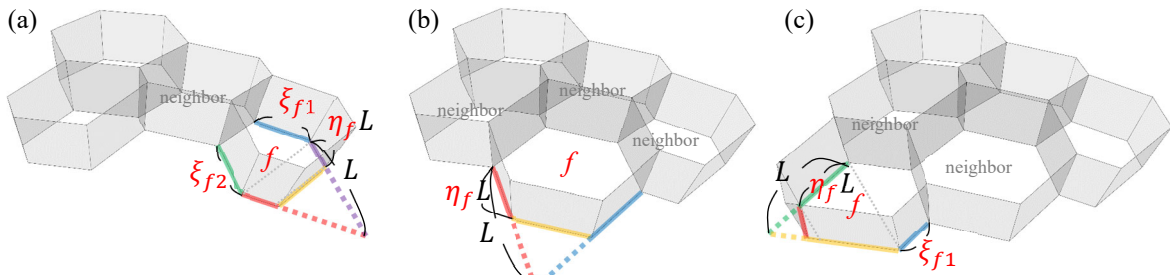


Figure 4. Sequential face generation of EO mesh M; (a) One neighboring face, (b) Three neighboring faces, (c) Two neighboring faces

In this paper, we consider only convex hexagonal faces for mesh M, meaning that the obtained mesh M can only approximate surfaces with positive Gaussian curvature. We believe that by appropriately constraining the direction and length of the edges for the new face $f$, this method could be extended to generate concave polygonal faces that approximate surfaces with negative Gaussian curvature. However, further investigation is needed to explore this extension, which will be addressed in future work.

Next, a method is described for adapting the shape of EO mesh M to the shape of a target surface $\Pi$, which is pre-specified by the designer, during the sequential addition of faces. Consider a set $F_g \subset F$ consisting of several faces within the EO mesh M. We formulate an optimization problem that collectively determines the shape of the faces included in the set $F_g$. Let $I_f$ denote the set of indices of

nodes on face $f$. The coordinates of node $i$ is denoted by $\boldsymbol{x}_i$. For each node $i$ on the added face $f$, the coordinates of nearest point $\hat{\boldsymbol{x}}_i$ on the target surface $\Pi$ and the unit normal vector $\hat{\boldsymbol{n}}_i$ at the same point are determined. The unit direction vector $\boldsymbol{n}_i = (\boldsymbol{x}_i' - \boldsymbol{x}_i)/\|\boldsymbol{x}_i' - \boldsymbol{x}_i\|$ of the node axis $A_i$ at the node $i$ of the EO mesh is defined by the referenced Koebe mesh $K$, and the following optimization problem is solved to minimize $\Phi_g$, the squared sum of the angle between $\boldsymbol{n}_i$ and the normal vector $\hat{\boldsymbol{n}}_i$ on the target surface.

(P)            minimize        $\Phi_g = \sum_{i \in I_f, f \in F_g} \|\boldsymbol{n}_i - \hat{\boldsymbol{n}}_i\|^2$

            subject to        $\|\boldsymbol{x}_i - \hat{\boldsymbol{x}}_i\| - D^U \leq 0 \quad (i \in I_f, f \in F_g)$

            $\eta_f^L \leq \eta_f \leq \eta_f^U, \qquad \xi_{f1}^L \leq \xi_{f1} \leq \xi_{f1}^U, \qquad \xi_{f2}^L \leq \xi_{f2} \leq \xi_{f2}^U$

Here, the number of variables is at most $|F_g| \times 3$, keeping the size of optimization problem small. The first constraint ensures that the difference between the coordinates of each node $\boldsymbol{x}_i$ of the EO mesh M and the nearest point $\hat{\boldsymbol{x}}_i$ on the target surface $\Pi$ is not more than the specified value $D^U$. In this study, the lattice shells represented by the EO mesh M and its offset mesh M' are referred to as *EO lattice shells*.
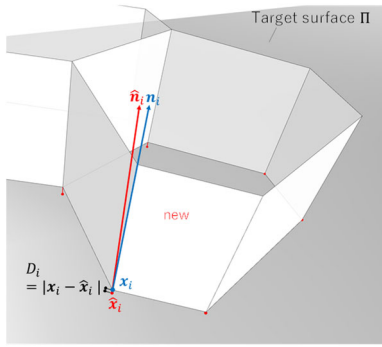


Figure 5. Distance $D_i$ between node $i$ and predetermined target surface $\Pi$
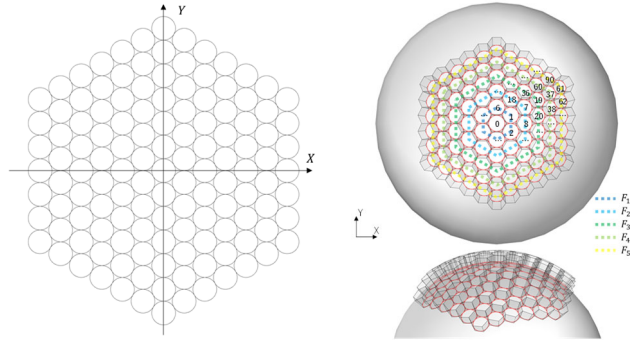
Figure 6. Base 2D circle pattern $P_0$ and the resulting Koebe mesh K

## 3. Numerical examples

### 3.1. Example 1: symmetric target surface with respect to two planes

As a numerical example, consider generating an EO mesh that conforms to the surface $\Pi$ as shown in Fig. 7 which is symmetric with respect to the *XZ* and *YZ* planes. The projection of this surface onto the *XY* plane is a square with sides of length $2l$, centered at $(0,0,0)$, with the *Z*-coordinates of the four corners, two points on the *XZ* plane, and two points on the *YZ* plane equal to $Z_D$, $Z_X$, and $Z_Y$, respectively. In the following examples, let $l = 5.0$.
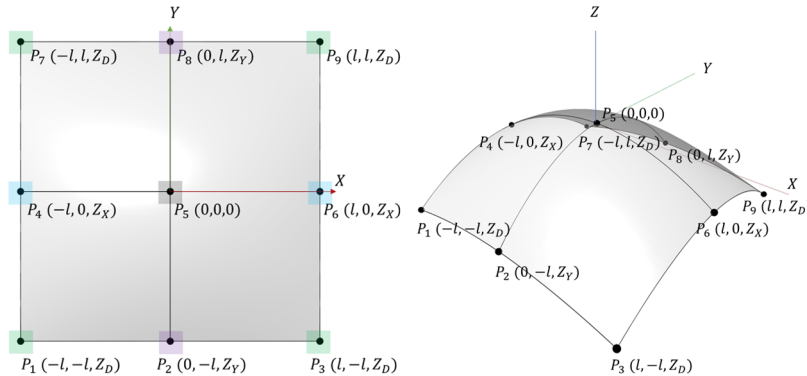


Figure 7. A target surface $\Pi$ symmetric with respect to the *XZ* and *YZ* planes

The Koebe mesh referenced in this example is obtained by $\alpha_R = \alpha_I = \beta_R = \beta_I = 0$ and $\rho = 3.0$ from the base circle pattern $P_0$ on the plane shown on the left in Fig. 6. The faces of this Koebe mesh are numbered sequentially from the center, and in a clockwise starting at 2 o'clock, as shown on the right of Fig. 6. All faces except for the first one are classified into sets $F_1 = \{1, \cdots, 6\}, F_2 = \{7, \cdots, 18\}, F_3 = \{19, \cdots, 36\}, F_4 = \{37, \cdots, 60\}, F_5 = \{61, \cdots, 90\}$, as shown on the right of Fig. 6. The initial face 0 is placed at the center $(0,0,0)$ of the target surface $\Pi$ due to geometric symmetry.

Considering the symmetry of the target surface and the referenced Koebe mesh K with respect to the *XZ* and *YZ* planes, the following equality constraints are taken into account during the solution of the optimization problem (P):

$$\left\| \widetilde{\boldsymbol{x}}_g - \boldsymbol{R}_{XZ}(\widetilde{\boldsymbol{x}}_g) \right\| + \left\| \widetilde{\boldsymbol{x}}_g - \boldsymbol{R}_{YZ}(\widetilde{\boldsymbol{x}}_g) \right\| = 0 \tag{3}$$

where $\widetilde{\boldsymbol{x}}_g$ is a vector composed of $18 \cdot |F_g|$ components, which are the coordinates of all the node sets $\{\boldsymbol{x}_i \in \mathbb{R}^3 \mid i \in I_f, f \in F_g\}$ included in the set of faces $F_g$. Then, $\boldsymbol{R}_{XZ}(\widetilde{\boldsymbol{x}}_g)$ is a vector obtained by swapping the node components of vector $\widetilde{\boldsymbol{x}}_g$ that are symmetrically positioned with respect to the *XZ* plane and by reversing the signs of the *Y*-coordinate components of all nodes. Similarly, $\boldsymbol{R}_{YZ}(\widetilde{\boldsymbol{x}}_g)$ is a vector obtained by swapping the node components of vector $\widetilde{\boldsymbol{x}}_g$ that are symmetrically positioned with respect to the *YZ* plane and by reversing the signs of the *X*-coordinate components of all nodes.

The shapes of the target surface $\Pi$ defined for various combinations of $Z_D, Z_X, Z_Y$, and the shapes of the obtained EO mesh M, are shown as CASES 1 to 3 in Fig. 8. Additionally, for reference, the shape of the EO mesh M when a spherical surface with a radius of 6.2 is specified as $\Pi$ is shown in Fig. 8 denoted as CASE 4. Here, the upper bound of the distance from each node of the initial face 0 to $\Pi$ is set as $D_0^U = 0.005$. The color contour on the target surface $\Pi$ represents Gaussian curvature, while the lines on the same surface indicate the directions of principal curvature. In this example, although $D^U$ is not specified, it can observed that in all cases the distance between each node of the generated mesh M and the target surface $\Pi$ is within 0.02, except beyond the outer edges of $\Pi$. This example shows that the proposed method allows us to obtain EO meshes that fit well with various specified surfaces.
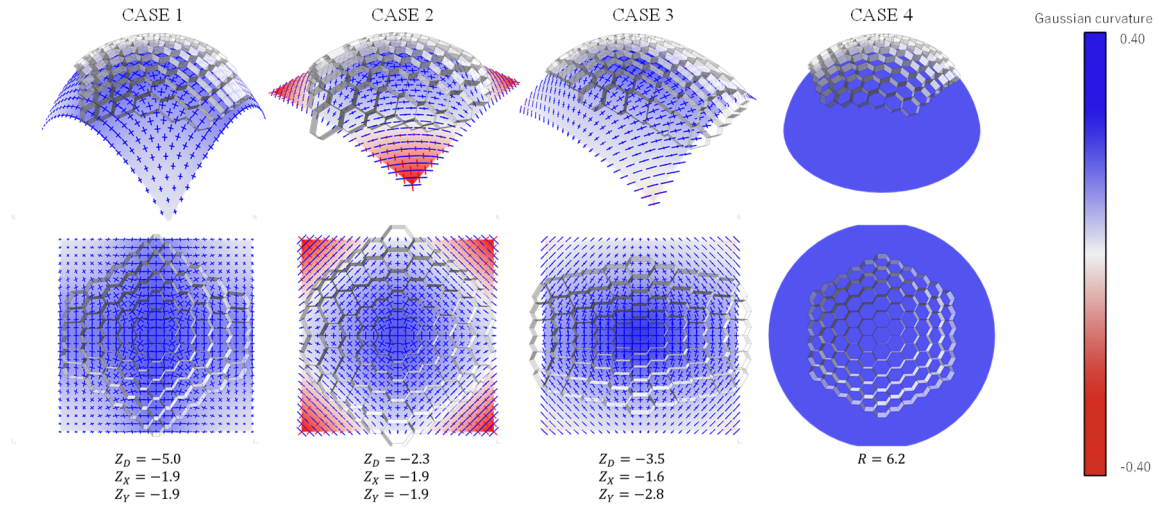


Figure 8. Result of numerical example 1

## 3.2. Example 2: EO lattice shells conforming to the shape of rotational surfaces

Next, consider an example targeting a rotational surface $\Pi$ around the *Z*-axis as shown in Fig. 9. The generatrix G of this rotational surface $\Pi$ is a cubic Bézier curve defined by four points on the *XZ* plane: Top point T, control points P and Q, and endpoint E. The normal vectors at points T and E on the generatrix G (and surface $\Pi$) are denoted as $\widehat{\boldsymbol{n}}_T$ and $\widehat{\boldsymbol{n}}_E$, respectively. Here, the coordinates of points T and E, as well as the normal vectors $\widehat{\boldsymbol{n}}_T$ and $\widehat{\boldsymbol{n}}_E$, are supposed to be specified as design conditions. Additionally, on the *XZ* plane, the intersection point R is determined by the line passing through T and

orthogonal to $\hat{\boldsymbol{n}}_T$ and the line passing through E and orthogonal to $\hat{\boldsymbol{n}}_E$, setting points P and Q such that $\overrightarrow{EP} = p\overrightarrow{ER}$ and $\overrightarrow{TQ} = q\overrightarrow{TR}$, where $p$ and $q$ are design parameters that define the shape of surface Π.

Here, given the coordinates of points T and E, and the directions of $\hat{\boldsymbol{n}}_T$ and $\hat{\boldsymbol{n}}_E$, we demonstrate a method to obtain an EO mesh that covers the outer edge and conforms to the shape of the surface Π with variable parameters $p$ and $q$. We discuss the relationship between the shape and mechanical properties of the lattice shell obtained from this method. In the following example, we set T(0,0,1.6), E(5,0,0), $\hat{\boldsymbol{n}}_T = (0, 0, 1)$, and $\hat{\boldsymbol{n}}_E = (\cos(\pi/3), 0, \sin(\pi/3))$. The shape and curvature distribution of the generatrix G for parameters $p = 0.40$ and $q = 0.70$, and the shape of surface Π, are shown in Fig. 9. Examples of the shape and curvature distribution of G and the corresponding shape of surface Π with varying parameters $p$ and $q$ are shown in Fig. 10. As seen from Fig. 10, a smaller parameter $p$ leads to a larger curvature near the outer point E, and a smaller $q$ leads to a larger curvature near the top point T.
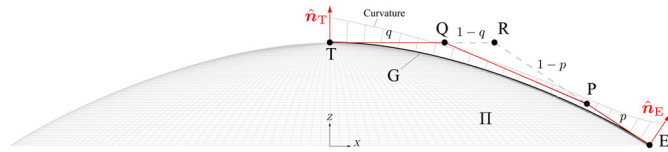


Figure 9. Revolute surface Π and its generatrix G
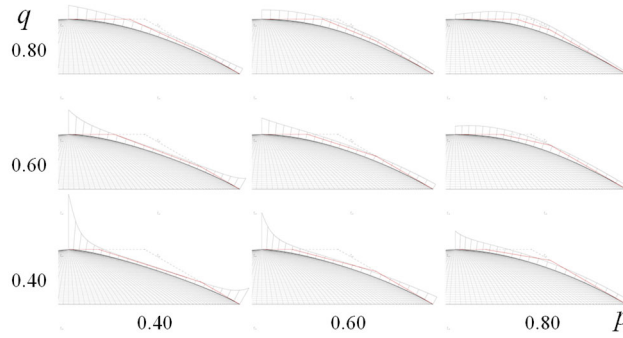


Figure 10. Shapes of generatrix G and surface Π obtained by various values at parameters $p$ and $q$

A base 2D circle pattern $P_0$, consisting of 61 units as shown in Fig. 11(a), possesses the same $D_6$ symmetry as a regular hexagon. When setting $\alpha_R = \alpha_I = \beta_R = \beta_I = 0$ among the five Möbius transformation parameters $\alpha_R, \alpha_I, \beta_R, \beta_I$ and $\rho$, the resulting Koebe mesh K (shown in Fig. 11(b)) and its parallel mesh, the generated EO mesh M, maintain $D_6$ symmetry with respect to the $Z$-axis. Furthermore, the node axis vectors at the outermost 12 nodes of the Koebe mesh K (indicated by arrows in Fig. 11(b)) are parallel to the node offset vectors at the outermost 12 nodes of the corresponding EO mesh M (shown by arrows in Fig. 11(c)). Therefore, by adjusting the remaining Möbius transformation parameter $\rho$ so that the angles formed by each of these 12 node offset vectors with the $Z$-axis are equal to the angle formed by vector $\hat{\boldsymbol{n}}_E$ (as shown in Figs. 9 and 11(c)) with the $Z$-axis, the value of $\rho$ that satisfies all these conditions can be found through iterative calculations, resulting in $\rho = 3.3648$. In the following, Koebe mesh K defined by this value is used.
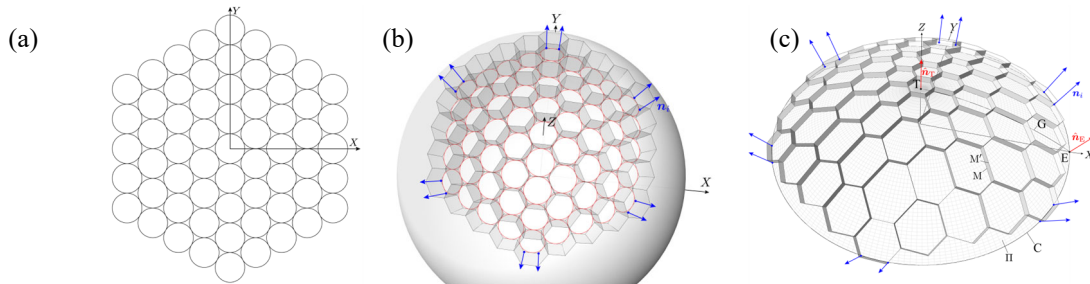


Figure 11. Generation of EO lattice shell: (a) Base 2D circle pattern $P_0$, (b) Koebe mesh K, (c) EO lattice shell consisting of EO mesh M and its offset mesh M′

The parameters $p$ and $q$ are varied with increments of 0.05 within the range of 0.4 to 0.8. Here, the beam height (the edge offset amount between EO mesh M and its offset mesh M') is set to 0.30, and the upper-bound distance $D^U$ between the nodes of the generated mesh and the target surface $\Pi$ is 0.10. To ensure that the outermost 12 nodes of EO mesh M reach the outermost circle C of surface $\Pi$ (shown in Fig. 11(c)), the sum of the squares of the distances between these nodes and circle C, multiplied by a positive weighting coefficient, is added to the objective function.

Examples of the obtained EO lattice for combination of $p$ and $q$ values in {0.4, 0.6, 0.8} are displayed in Fig. 12. As observed in Fig. 12, a smaller value of $p$ (a larger curvature at the outer edge) leads to a shorter edge lengths of the faces near the outer edge, resulting in denser faces. Similarly, a smaller value of $q$ (a larger curvature at the top) leads to a shorter edge lengths of the faces near the top, also resulting in denser faces.



(a) Perspective view          (b) Top view
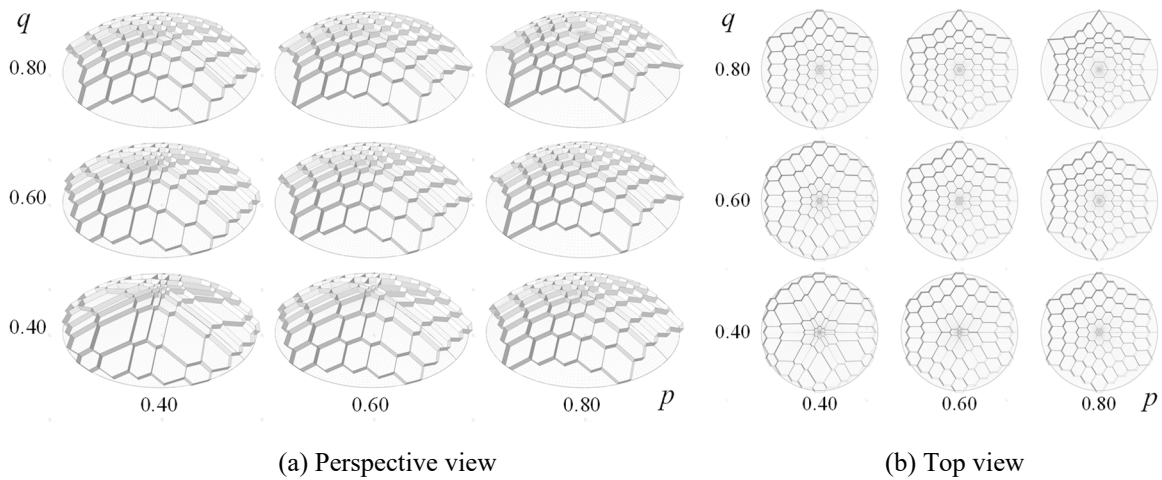
Figure 12. Variation of shape of the EO lattice shell with respect to parameters $p$ and $q$

The structural performance of the generated EO lattice shell is verified through structural analysis. An example of the analysis model is shown in Fig. 13(a). Each beam of the lattice shell has a rectangular cross-section and is modeled with shell elements made up of triangular elements obtained by diagonally dividing a quadrilateral, which is created by dividing the beam height direction into 6 parts and the length direction into 16 parts. The beam height is equal to the edge offset amount of 0.300 [m], and the thickness is 0.006 [m]. A concentrated load 1.0 [kN] is applied in the negative $Z$-axis direction at each node of the offset mesh M', which is the intersection points at the top edges of each face. For the support conditions, the outermost 12 nodes of mesh M, which are the intersection points at the bottom edges of each beam, are simply supported. To avoid in-plane deformation of each face, beam elements with a hollow circular cross-section (referred to as *face reinforcement elements* in this study), with a diameter of 0.030 [m] and thickness of 0.005 [m], are placed to connect each node within the same face and their centroid on both mesh M and offset mesh M'. The face reinforcement elements are rigidly connected at the centroid and pinned at the nodes of mesh M and offset mesh M', respectively.

Additionally, for the surface $\Pi$ and EO lattice shell defined by each set of $(p, q)$, a comparison is made with a lattice shell (hereafter, *non-EO lattice shell*) shown in Fig. 13(b), which does not meet the characteristics of an EO mesh adapted to the same surface $\Pi$. This non-EO lattice shell is defined by projecting uniform regular hexagons, filled in the plane to fit within circle C at the outer edge and having the same number as the EO lattice shell, vertically onto surface $\Pi$ to determine the coordinates of nodes $\boldsymbol{x}_i$ of mesh M, with the coordinates of corresponding offset nodes $\boldsymbol{x}_i' = \boldsymbol{x}_i + h\boldsymbol{n}_i$. Here, $\boldsymbol{n}_i$ is the normal vector of surface $\Pi$ at $\boldsymbol{x}_i$, and $h$ is set to the average value of $\|\boldsymbol{x}_i' - \boldsymbol{x}_i\|$ for the corresponding EO lattice shell. In this case, the bottom edge $e_{ij}$ and the top edge $e_{ij}'$ of the beam $ij$ in the central plane of the non-EO lattice shell are not parallel but are in a twisted position relative to each other (see Fig. 14). As indicators of the degree of this twist, consider $e_{\text{thick}}$ and $e_{\text{height}}$ as shown in Fig. 14, where $e_{\text{thick}}$ represents the distance from the perpendicularly projected point from $\boldsymbol{x}_j'$ to the plane spanned by $\boldsymbol{x}_i, \boldsymbol{x}_i', \boldsymbol{x}_j'$, and $e_{\text{height}}$ represents the distance between the same point and a line parallel to $e_{ij}$ passing

through $x_i'$. The material properties for all the lattice beam shell elements are Young's modulus $E = 2.10 \times 10^5$ [N/mm²], shear modulus $G = 8.076 \times 10^4$ [N/mm²], and for the face reinforcement elements, these values are multiplied by 100. Structural analysis was conducted using Karamba 3D [4].

When varying parameters $p$ and $q$, the total mass of the lattice beams for both the EO lattice model and the non-EO lattice model, the maximum value of the distance $D_i$ between the nodes of mesh M and surface $\Pi$, and the maximum values of $e_{\text{thick}}$ and $e_{\text{height}}$ are shown in Figs. 15(a)-(d), respectively. As indicated in Fig. 15(a), the total mass of the EO lattice decreases as both $p$ and $q$ increase. As shown in Fig. 15(b), the maximum value of $D_i$ shows a valley at intermediate values of $p$ and $q$. Even in the case that shows the maximum value, 0.0575, at $(p, q) = (0.4, 0.4)$, it is confirmed that an EO lattice shell fitting the designated surface is obtained in all cases. Furthermore, as shown in Figs. 15(c) and (d), it is observed that in the non-EO lattice shell, $e_{\text{thick}}$ and $e_{\text{height}}$ do not become zero, indicating that twisting occurs in the beams.

(a)

(b)
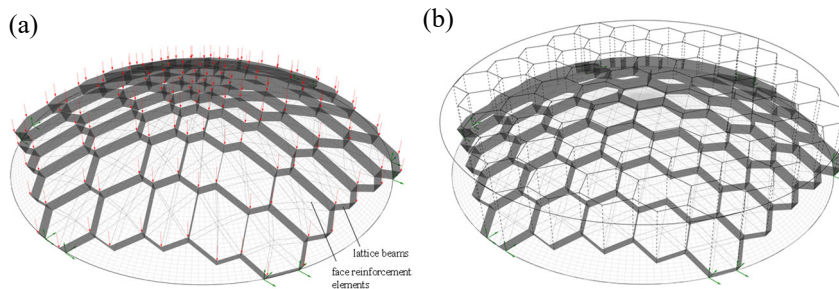


Figure 13. Analysis model: (a) EO lattice model, (b) Non-EO lattice model
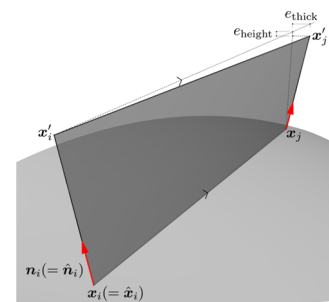
Figure 14. Deviations $e_{\text{thick}}$ and $e_{\text{height}}$ of lattice beams in the non-EO model



(a) Total mass

(b) Max. value of $D_i$

(c) Max. value of $e_{\text{thick}}$

(d) Max. value of $e_{\text{height}}$
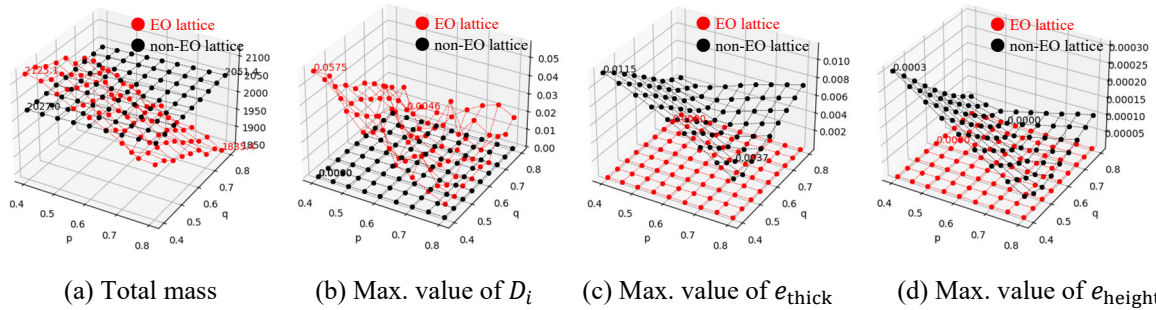
Figure 15. Shape analysis result: (a) Total mass of lattice beams [kg], (b) maximum distance between nodes and target surface [m], (c) Maximum deviation $e_{\text{thick}}$ in the thickness direction [m], (d) Maximum deviation $e_{\text{height}}$ of beam height [m]



(a) Elastic energy [kN · m]

(b) Average of $|N_x|$ [kN/m]

(c) Average of $|M_{xx}|$ [kN · m/m]
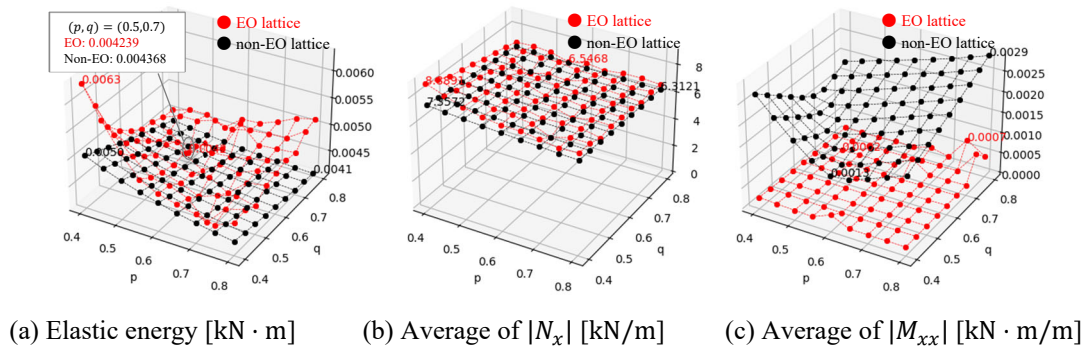
Figure 16. Structural analysis result

Similarly, Fig. 16(a) shows the elastic strain energy [kN · m] for both the EO lattice shell and the non-EO lattice shell, and Figs. 16(b) and (c) display the average values of the absolute total force in the beam axis (*x*-axis) direction, $|N_x| = \left| \int_{-t/2}^{t/2} \sigma_{xx} dz \right|$ [kN/m], and the absolute value of the total bending moment in the *x*-axis direction, $|M_{xx}| = \left| \int_{-t/2}^{t/2} \sigma_{xx} \cdot z \, dz \right|$ [kN · m/m], for each shell element of the lattice beams. Here, $\sigma_{xx}$ represents the normal stress in the *x*-direction for each shell element, the *z*-axis denotes the axis perpendicular to the face (thickness direction), and *t* represents the thickness of lattice beams. From Fig. 16(a), it is observed that the elastic strain energy of the EO lattice shell generally has a convex distribution, and the minimum value of 0.004239 exists at $(p,q) = (0.5,0.7)$, which is smaller than the elastic strain energy of the non-EO lattice shell, 0.004368, for the same $(p,q)$. Furthermore, as shown in Fig. 16(b), there is no significant difference in the average value of the axial forces generated in each lattice beam between the EO and non-EO lattice shells. However, as illustrated in Fig. 16(c), the bending moment around the weak axis in each lattice beam in the non-EO lattice shells is significantly larger than that of the EO lattice shells. This may be due to the presence of the twist-induced deviation $e_{\text{thick}}$ in the non-EO lattice shells, as mentioned earlier.

As shown in Fig. 16(a), the maximum elastic strain energy of the EO lattice shell occurs at $(p,q) = (0.40, 0.40)$, while the minimum occurs at $(p,q) = (0.50, 0.70)$. The shapes at these points are shown in Figs. 17(a) and 17(b), respectively. Compared to Fig. 17(a), the shape as shown in Fig. 17(b), where the elastic strain energy is minimal, shows a more balanced distribution of edge lengths among the faces. Furthermore, Fig. 17(c) shows the shape of the non-EO lattice shell corresponding to the same $(p,q)$ and surface Π as of Fig. 17(b).



(a) EO lattice (Max. strain energy)
$(p,q) = (0.40, 0.40)$
$E = 0.006344$

(b) EO lattice (Min. strain energy)
$(p,q) = (0.50, 0.70)$
$E = 0.004239$

(c) Non-EO lattice
$(p,q) = (0.50, 0.70)$
$E = 0.004368$
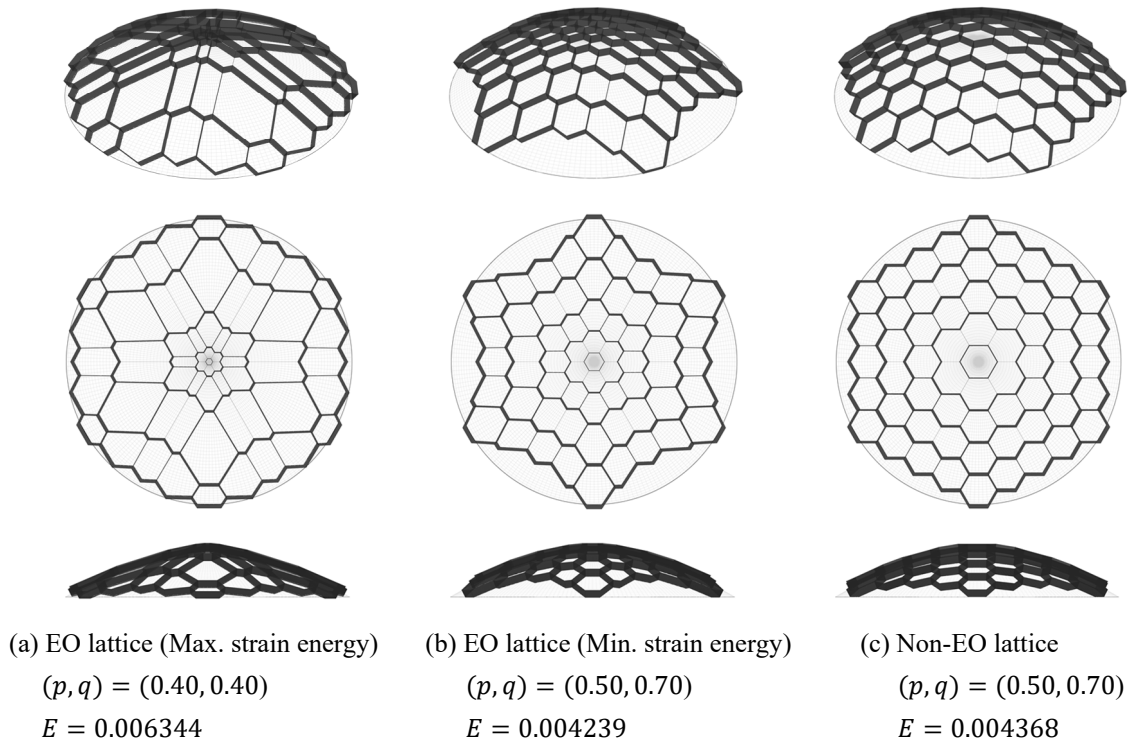
Figure 17. Shapes of the surface Π and the obtained EO and non-EO lattice shell

Deformation of the lattice beams of the EO lattice shell and the non-EO lattice shell are presented in Figs. 18(a) and (b), respectively. From these figures, it is observed that the non-EO lattice shell in Fig. 18(b) exhibits significant weak-axis bending deformation compared to the EO lattice shell as shown in Fig. 18(a). This is due to the relatively large weak-axis bending moments $|M_{xx}|$ (shown in Fig. 16(c)) generated in the lattice beams of the non-EO lattice shell, caused by the previously mentioned $e_{\text{thick}}$. This weak-axis bending deformation not only causes additional stress to the lattice beams but also is considered to potentially lead to detachment or damage of the finishing materials applied to each surface. In the EO lattice shell, this weak-axis bending deformation is relatively suppressed, as can be seen from Fig. 18(a).

| (a) EO lattice beams | (b) Non-EO lattice beams |
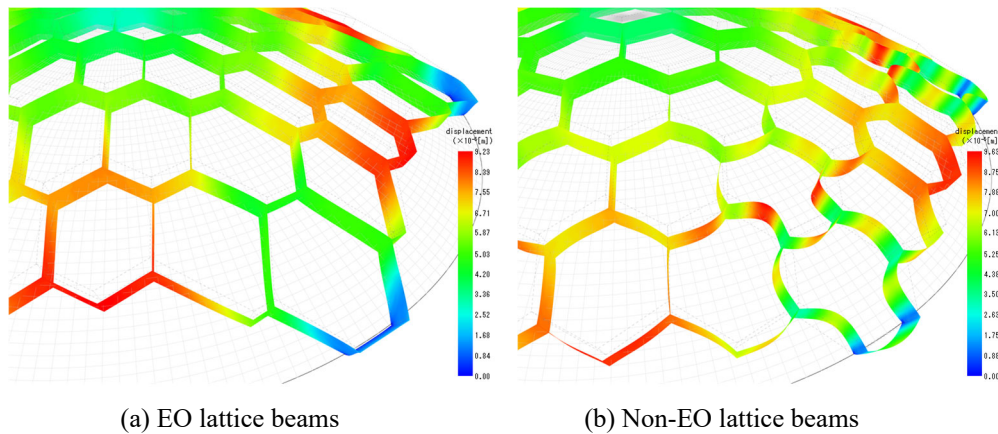
Figure 18. Deformation of the two models for $(p, q) = (0.50, 0.70)$ (magnification factor: 2000)

## 4. Conclusion

In this study, we proposed a method to find hexagonal lattice shells that conform to a specified surface shape using sequential optimization, ensuring that joints do not twist, each face maintains planarity, and the shell consists only of beams with uniform height. The proposed method determines the EO mesh by minimizing the angle between the node axis of the EO mesh and the normal at the nearest point on the specified surface.

The method proposed in this study was applied to multiple surfaces with positive Gaussian curvature, confirming the effectiveness of our approach through the first numerical example. From this example, we showed that the proposed method allows us to obtain EO meshes that fit well with various specified surfaces. The proposed method is thought to be extendable to surfaces with negative Gaussian curvature by reversing the direction of some edges to generate concave polygons. However, this extension will be a subject for future investigation.

Secondly, by applying this method to rotational surfaces, we demonstrated that it is possible to determine shapes of EO lattice shells that satisfy the properties of EO meshes while exhibiting enhanced structural performance. We also examined the differences in mechanical properties between lattice shells that do and do not satisfy the properties of EO meshes. The non-EO lattice shells might cause issues such as the detachment or damage of finishing materials applied to each face, due to weak-axis bending induced by misalignments at both ends of the beam axis. In contrast, it was shown through structural analysis that the EO lattice shells effectively suppress this weak-axis bending deformation.

## Acknowledgements

## References

[1]  H. Pottmann, Y. Liu, J. Wallner, A. Bobenko and W. Wang, "Geometry of multi-layer freeform structures for architecture," *ACM SIGGRAPH 2007 papers,* pp. 65–es, 2007.

[2]  A. I. Bobenko, P. Schröder, J. M. Sullivan and G. M. Ziegler, *Discrete Differential Geometry*, Oberwolfach Seminars, Vol. 38, Birkhaeuser, 2008.

[3]  R. Watada and M. Ohsaki, "Shape generation of hexagonal lattice shell consisting of edge offset mesh," *Proceedings of IASS Annual Symposia 2023,* No. 24, pp. 1–7, 2023.

[4]  C. Presinger, "Linking Structure and Parametric Geometry," *Architectural Design,* vol. 83, pp. 110-113, 2013.